THE JOURNAL OF PHYSICAL CHEMISTRY C

Article

pubs.acs.org/JPCC

Influence of Cationic Precursors on CdS Quantum-Dot-Sensitized Solar Cell Prepared by Successive Ionic Layer Adsorption and Reaction

Ru Zhou,[†,‡] Qifeng Zhang,[†] Jianjun Tian,[†] Daniel Myers,[†] Min Yin,*[,‡] and Guozhong Cao*[,†]

[†]Department of Materials Science and Engineering, University of Washington, Seattle, Washington 98195, United States

[‡]Department of Physics, University of Science and Technology of China, Hefei 230026, China

Supporting Information

ABSTRACT: Successive ionic layer adsorption and reaction (SILAR) is the most extensively used method for the direct and simultaneous synthesis and deposition of quantum dots (QDs) onto porous oxide films for quantum-dot-sensitized solar cell (QDSC) applications. In this work, the noticeable influences of the cationic precursors on the deposition of CdS QDs and the QDSC performance have been studied. A careful comparison of two cationic precursors, cadmium nitrate and cadmium acetate, for the preparation of CdS QDSCs by the SILAR method showed that, compared to the commonly used cadmium nitrate, cadmium acetate provided a significantly higher deposition rate of CdS QDs on TiO_2 films. A solar cell power conversion efficiency of 2.15% was achieved for a CdS QDSC employing cadmium acetate as the cationic precursor, much higher than the value of 1.44% obtained for the cell prepared using cadmium nitrate for the same number of SILAR cycles. Control experiments in which the recipes of the cationic precursor solutions were changed revealed a dramatic effect of the cationic precursor pH on the deposition rate of CdS QDs on the TiO_2 film. In addition, an appreciable anomalous red shift, which became more pronounced with increasing amount of QDs, was observed in both the optical absorption and photocurrent spectra of CdS-sensitized TiO_2 films.

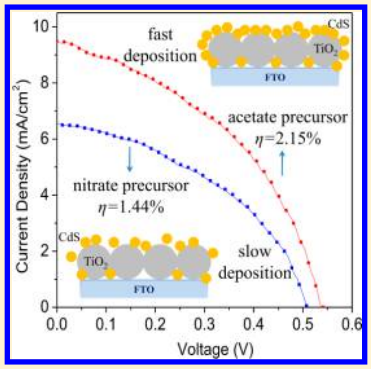

1. INTRODUCTION

Over the past two decades, research on sensitized solar cells has grown significantly, and the technology has been considered as one of the most cost-effective alternatives to the silicon and other semiconductor-based photovoltaic devices because of the low-cost and simple fabrication process.[1−6] Recently, a record solar-to-electricity conversion efficiency as high as 15% was achieved for perovskite-sensitized solar cells.[7] As a derivative of dye-sensitized solar cells (DSCs), quantum-dot-sensitized solar cells (QDSCs) are now attracting tremendous attention because of the extraordinary optical and electrical properties of QDs, such as band gaps tunable across wide energy ranges, strong light absorption, high stability against oxidative deterioration, high extinction coefficients, and large intrinsic dipole moments facilitating charge separation.[8−11] Although there have been quite a few studies on the application of QDs, such as CdS,[12−19] CdSe,[20−22] PbS,[23,24] and Ag_2S[25,26] QDs, as sensitizers for light harvesting in solar cells, the performance of QDSCs, typically with power conversion efficiencies in the range of 1−5%, still lags much behind those of DSCs. Among various semiconductors used for QDSCs, CdS/CdSe-QD-cosensitized solar cells are most attractive and recently have been reported to achieve power conversion efficiencies as high as 5% based on mesoscopic TiO_2 films.[27,28] To further improve the performance of QDSCs, one of the urgent issues is to determine the difficulty of assembling QDs effectively in mesoporous TiO_2 or ZnO films to obtain a fully covered layer of QDs on the TiO_2 or ZnO surface.

Two methods have been widely employed and extensively studied for the assembly of QDs. One is in situ growth of the QDs on a mesoporous oxide, for example, TiO_2 or ZnO, including successive ionic layer adsorption and reaction (SILAR)[10−15,17−19,29] and chemical bath deposition (CBD).[10,11,30] The other is self-assembled binding of presynthesized QDs on the surface of an oxide through the link of bifunctional molecules [i.e., self-assembled monolayer (SAM) technique].[20,31] Although the SAM technique has the advantage of providing precise control of the size of the QDs, it is difficult to achieve uniform and sufficient coverage of the QDs on the oxide film.[20,32] In addition, the use of a SAM complicates the charge-transfer process from the QDs to the oxide. To date, SILAR, which deposits various light-absorbing QDs in mesoporous oxides through the direct in situ surface adsorption of ions, has been the most common method employed for making QDSCs. In the SILAR process, to deposit the semiconductor QDs in mesoporous films, the films are dipped, in sequence, into aqueous precursor solutions of the reactants. Ions of the reactants penetrate into the mesoporous film and incorporate into the interior of the mesopores. The

Received: October 27, 2013
Revised: November 26, 2013
Published: December 5, 2013

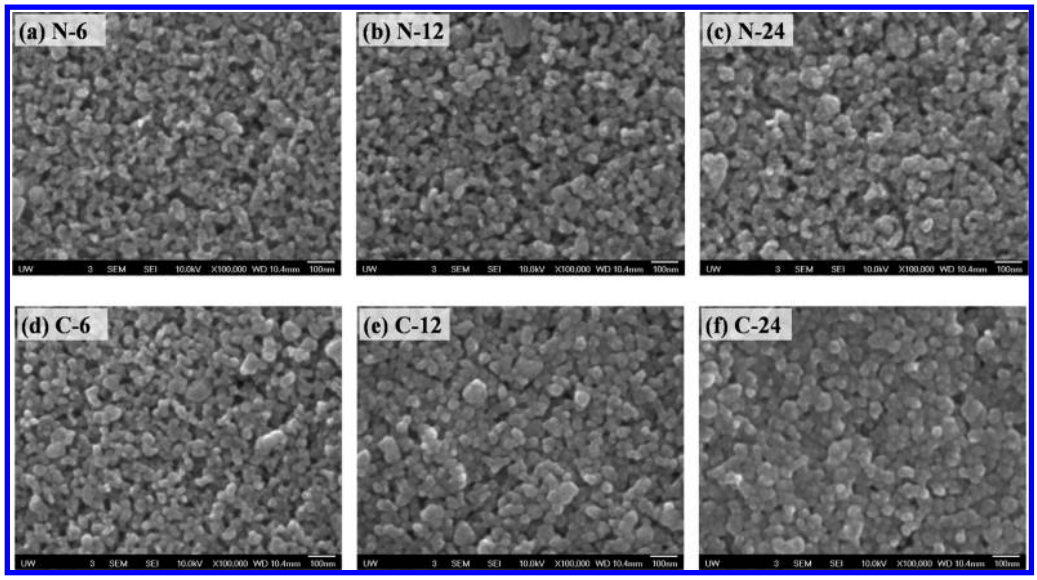

Figure 1. SEM images of CdS-deposited TiO_2 films prepared for different numbers of SILAR cycles [(a,d) 6, (b,e) 12, and (c,f) 24] using (a−c) $Cd(NO_3)_2$ and (d−f) $Cd(Ac)_2$ as the cationic precursors.

ions that are adsorbed during the first dip react with ions of the opposite charge during the second dip, leading to the formation of one molecular layer of the semiconductor. The process is repeated until the desired thickness is obtained.

CdS is one of the most commonly used semiconductors for QDSCs. To form CdS QDs through the SILAR method, two kinds of precursor ions, namely, Cd^{2+} and S^{2-}, are adsorbed onto the surface of TiO_2 nanoparticles sequentially. In the literature, for the deposition of CdS QDs by the SILAR method, cadmium nitrate [$Cd(NO_3)_2$] is usually used as the Cd^{2+} source[10−14,17−19,27,28] with sodium sulfide (Na_2S) as the anion (S^{2-}) source, whereas cadmium acetate [$Cd(Ac)_2$] has rarely been employed. To our knowledge, only the Mora-Seró group recently reported the use of acetate salts to deposit QDs by SILAR, and they found that a higher cell performance could be obtained when the acetate precursor was employed for electrode sensitization compared to nitrate precursor.[33,34] Rabinovich and Hodes, who used $Cd(Ac)_2$ in 50% methanol/water as the precursor for the preparation of CdS films, studied the anomalous red-shift effect of CdS but did not investigate the cell performance.[35] In this study, through a detailed comparison of the influence of $Cd(NO_3)_2$ and $Cd(Ac)_2$ precursors on the CdS QD deposition rate and cell performance, we found that the difference in pH values of the precursor solutions might be responsible for the appreciable influence of the precursors on CdS QDSCs prepared by SILAR. Control experiments in which the recipes of cationic precursor solutions for CdS QD deposition were changed were carefully carried out to provide evidence for this conclusion, which has not been reported before.

2. EXPERIMENTAL SECTION

2.1. Preparation of Mesoporous TiO_2 Films. Commercially available F-doped tin oxide (FTO) glass was used as transparent conducting substrates for the preparation of TiO_2 photoanodes. Mesoscopic TiO_2 films were prepared by doctor blading TiO_2 paste (Degussa P25) onto the substrate and then sintering at 500 °C for 30 min in air at a heating rate of 5 °C/min. The thickness of the TiO_2 film, measured from a cross-sectional scanning electron microscopy (SEM) image, was about 9 μm. The active area of the TiO_2 films was approximately 0.36 cm^2 (0.6 cm × 0.6 cm).

2.2. Fabrication of CdS QD-Sensitized Photoanodes. To synthesize and assemble CdS QDs on TiO_2 films, the substrate was sequentially immersed in solutions of Cd^{2+} and then S^{2-}, and the sample was rinsed with methanol between each dip. The purpose of the rinsing step was to remove excess ions, which hinder the formation of the desired monolayer adsorption. The cationic precursors (Cd^{2+} and Zn^{2+}) were based on methanol solutions, whereas a solvent including water and methanol (1:1, volume ratio) was employed for the anionic precursors (S^{2-}). For the sake of direct comparison, $Cd(NO_3)_2$ and $Cd(Ac)_2$ methanol precursors with the same concentration of 0.1 M were used as the Cd^{2+} sources. First, the TiO_2 films were immersed in $Cd(NO_3)_2$ or $Cd(Ac)_2$ precursor for 1 min, rinsed with methanol, and dried in air. Then, the films were dipped into a 0.1 M Na_2S precursor for 1 min to allow S^{2-} to react with the preadsorbed Cd^{2+}. Afterward, the electrodes were again rinsed with methanol and dried. The two-step dipping procedure is defined as one SILAR cycle. The incorporated amount of CdS QDs can be increased by repeating the SILAR cycle. To improve the stability and performance, all SILAR electrodes were covered with a ZnS passivation layer at the end, by being dipped twice alternately in 0.1 M $Zn(Ac)_2$ and 0.1 M Na_2S solutions for 1 min per dip.

2.3. Preparation of Electrolyte and Counter Electrode. The electrolyte employed in this study was composed of 1 M S and 1 M Na_2S in deionized water. The counter electrode was a Cu_2S film fabricated on a brass foil. The preparation of the Cu_2S electrode followed the procedure reported in the literature[10,11] and can be described briefly as follows: Brass foil was immersed in 37% hydrochloric acid (HCl) solution at about 70 °C for 30 min, then rinsed with water, and dried in air. After that, the etched brass foil was dipped into 1 M S and 1 M Na_2S aqueous solution for about 5 min, resulting in the formation of a black Cu_2S layer on the foil. The solar cells were prepared by sandwiching the Cu_2S counter electrode and QD-sensitized photoanode using a scotch tape spacer (~50 μm in thickness) and permeating the assembly with polysulfide electrolyte.

dx.doi.org/10.1021/jp410615b | J. Phys. Chem. C 2013, 117, 26948−26956

2.4. Characterization of Materials and QDSCs. The morphologies of the film samples were characterized by scanning electron microscopy (SEM, Philips, JEOL JSM 7000). Energy-dispersion X-ray (EDX) analysis was used to analyze the element contents and distribution. At least three areas (~100 μm^2) on the film surface (~1.5 cm^2) were randomly selected for EDX measurements on each sample. Optical absorption spectra were measured on a Thermo Scientific UV−vis−NIR spectrophotometer (Evolution 300 PC) fitted with an integrating sphere. The photovoltaic properties were measured using an HP 4155A programmable semiconductor parameter analyzer under AM 1.5 simulated sunlight with a power density of 100 mW/cm^2. The incident-photon-to-carrier conversion efficiency (IPCE) was determined by taking the ratio of the device photocurrent to the photocurrent of a Si photodiode with a known spectral response, and the samples were illuminated by a 75-W xenon lamp (Spectra Physics model 60100) filtered by a monochromator (Acton Spectra Pro 2150i). The pH values were measured with a VWR symphony meter.

3. RESULTS AND DISCUSSION

Samples obtained employing $Cd(NO_3)_2$ and $Cd(Ac)_2$ as the Cd^{2+} precursors for different numbers of SILAR cycles are denoted as N-*m* (*m* = 6, 12, and 24) and C-*n* (*n* = 6, 12, and 24), respectively (where *m* and *n* represent the numbers of SILAR cycles). The mesoporous structure of TiO_2 films favors the penetration of the cationic and anionic precursor solutions. Figure 1 shows the morphologies of CdS-deposited TiO_2 films obtained using $Cd(NO_3)_2$ and $Cd(Ac)_2$ as Cd^{2+} sources. For both series, N-*m* and C-*n*, the surface of the films became more compact with increasing number of SILAR cycles, suggesting that increased amounts of CdS QDs were deposited onto the TiO_2 film. In comparison with the N series, a higher coverage of QDs on the TiO_2 surface was likely obtained for the C series for the same number of SILAR cycles, as more pores on the film surface were filled by the larger number of QDs deposited. In other words, $Cd(Ac)_2$ as the Cd^{2+} source appeared to result in a higher deposition rate than $Cd(NO_3)_2$. From the SEM images, it is obvious that the small pores on the films were partially blocked for large numbers of SILAR cycles, especially as shown for sample C-24 (Figure 1f).

The relative amount of CdS QDs adsorbed on the film was examined by EDX analysis. EDX spectra of pure TiO_2 and CdS-sensitized films are presented in Figure S1 of the Supporting Information. As shown, the pure TiO_2 film exhibited only the two typical peaks corresponding to Ti and O, whereas for the CdS-sensitized TiO_2 films, energy-dispersion peaks corresponding to Cd and S also appeared. The stronger peak intensities of Cd and S indicated a larger amount of CdS QDs adsorbed. Figure 2 presents the atomic ratios of Cd and S in the variuos samples based on EDX calculations. Obviously, more CdS QDs were deposited on the films for the C series than for the N series for the same number of SILAR cycles. This is consistent with the results reflected in the SEM images, which showed a higher coverage of QDs on the TiO_2 surface for the C series. In addition, it reveals that, in these films, the amount of Cd was slightly higher than the amount of S, suggesting there might exist extra Cd (or S deficiency) in the TiO_2 films. Similar results (i.e., excess Cd) have also been reported for CdS nanoparticles and CdS-sensitized ZnO films.[35,36] Cross-sectional images with EDX analyses (Figure S2, Supporting Information) revealed that the distributions of Cd and S were essentially homogeneous throughout the thickness of the mesoporous TiO_2 films.

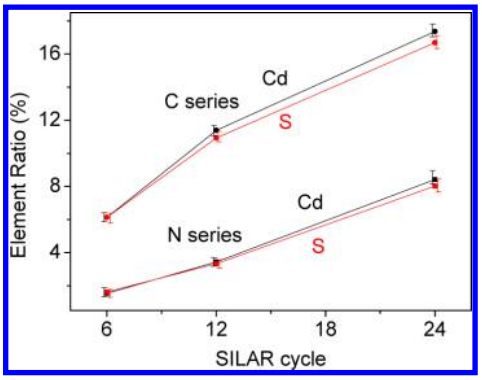

Figure 2. Element ratios of Cd and S based on EDX calculations for CdS-deposited TiO_2 films prepared for different numbers of SILAR cycles.

An absorption red shift for CdS deposited by SILAR was observed. From the absorption spectra in Figure 3a,b for samples from both the N and C series, it can be seen that the optical absorption edge shifted to longer wavelength with increasing number of SILAR cycles, although a slight blue shift was also observed for sample N-6 in a few initial cycles as a result of the quantum confinement effect of QDs.[37] As the number of cycles increased, the shift of the absorption edge became increasingly pronounced, with the corresponding band gap smaller than that of bulk CdS (as shown for the films except N-6), as discussed further in the following paragraphs. The red shift was also verified by the color change of the sensitized TiO_2 films as the QD deposition proceeded (Figure S3, Supporting Information). The change in color occurred much more quickly in the films of the C series than in those of the N series.

It is well-known that the optical band gap (E_g) for direct interband transitions and the absorption coefficient (A) near the absorption edge exhibit a relationship of the form[10,38]

$$(Ah\upsilon)^2 = c(h\upsilon - E_g) \quad (1)$$

where c is a constant, υ is the frequency, and h is Planck's constant. The optical band gap can be obtained by extrapolating the linear portion of a plot of $(Ah\upsilon)^2$ versus $h\upsilon$ at $A = 0$.

According to the $(Ah\upsilon)^2$ versus $h\upsilon$ plots in Figure 3c,d, the calculated band gaps of the CdS QDs are considerably lower than the band gap of bulk CdS (as depicted by the vertical dashed line at 2.42 eV) except for that of N-6. The eventual estimated effective band gaps and the band-gap red shift, ΔE, are reported in Table 1. As increased numbers of SILAR cycles directly resulted in increased amounts of QDs adsorbed on the TiO_2 film, this implies that the red shift is closely related to the increased amount of QDs (Figure S4a, Supporting Information). For the same number of SILAR cycles, the much more pronounced shift observed for the C series than for the N series should be attributed to the higher deposition rate achieved using $Cd(Ac)_2$ as the cationic precursor, which resulted in more QDs attached to the film. Sample C-24 exhibited an effective band gap of 2.03 eV, shifted as much as 0.39 eV (~16%) beyond the band gap of bulk CdS, 2.42 eV. This red shift is larger than the values reported in the literature for both SILAR- and CBD-deposited CdS.[12,13,35,37,39,40]

dx.doi.org/10.1021/jp410615b | J. Phys. Chem. C 2013, 117, 26948−26956

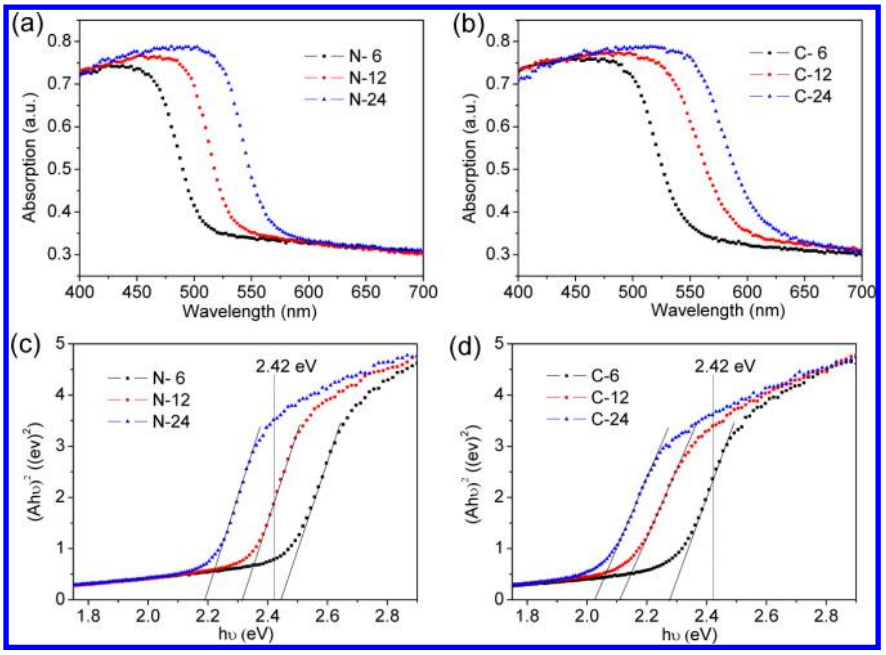

Figure 3. (a,b) UV−vis absorption spectra of CdS-sensitized TiO_2 films prepared for different numbers of SILAR cycles. (c,d) $(Ah\upsilon)^2$ vs $h\upsilon$ plots for determining the absorption onsets of the films. The vertical dashed line at 2.42 eV indicates the band-gap value of bulk CdS.

Table 1. Band Gaps, Absorption Onsets, and Band-Gap Shifts of CdS QDs Prepared for Different Numbers of SILAR Cycles

sample	absorption onset (nm)	effective band gap (eV)	ΔE^a (eV)
N-6	508	2.44	−0.02
N-12	537	2.31	0.11
N-24	566	2.19	0.23
C-6	546	2.27	0.15
C-12	590	2.10	0.32
C-24	611	2.03	0.39

[a]Band-gap shift with respect to that of bulk CdS (2.42 eV).

Even though this anomalous absorption-edge red shift has been reported in many publications,[12,13,35,37,39,40] a well-established and generally accepted explanation of the cause of this phenomenon is still lacking. Recently, Rabinovich and Hodes studied the red-shift phenomenon appearing in the optical spectra of CdS deposited by SILAR onto ZnO nanorods and concluded that the red shift is unlikely to be due to a lower band gap but seems to result from a particularly long absorption tail that extends far into the red region and is amplified by the large optical thickness of high-surface-area nanoporous films.[35] As the number of the SILAR cycles increased (as did the amount of CdS QDs), a greater red shift was observed. A high degree of structural disorder that could localize states near the band gap in CdS QDs might be one explanation for such pronounced tailing. Another explanation comes from a study based on CdS nanorods and nanocages in which Tong et al. estimated E_g to be as low as 2.18 eV.[36] It is suggested that the electronic coupling of interfacial Cd−Cd pairs could bring about a self-narrowed band gap for an assembly of CdS nanocrystals compared to individual CdS nanocrystals and bulk CdS material. Such a hybridization of the Cd levels in Cd-rich (or S-deficient) CdS could create new energy levels inside the original band gap that were responsible for the lower-energy transition. This argument was supported by experimental data revealing a Cd excess compared to S (Cd:S = 1.17) and was further verified by an electronic structure calculation. In our study, a Cd excess was also found in SILAR-deposited CdS, and almost all of the samples exhibited a slightly higher atomic content of Cd than S, as evidenced by the results of EDX calculations shown in Figure 2b.

The photovoltaic characteristics of the CdS QDSCs under one-sun illumination (AM 1.5 G, 100 mW/cm^2) are presented

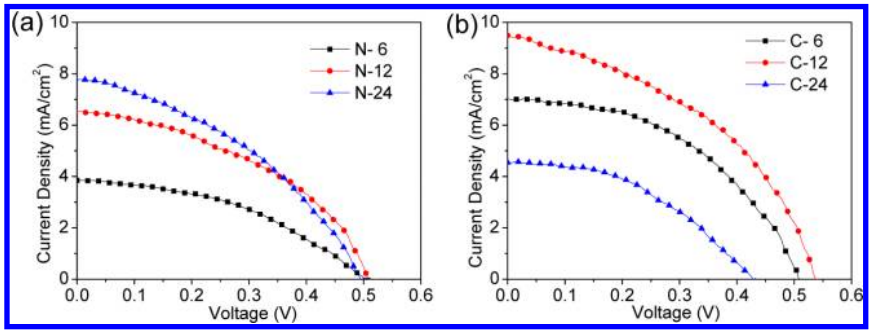

Figure 4. $J-V$ characteristics of various CdS QDSCs measured under the illumination of one sun (AM 1.5, 100 mW/cm^2).

dx.doi.org/10.1021/jp410615b | J. Phys. Chem. C 2013, 117, 26948−26956

in panels a and b of Figure 4 for the N and C series, respectively. The short-circuit current (J_{sc}), open-circuit voltage (V_{oc}), fill factor (FF), and power conversion efficiency (η) are summarized in Table 2. For each type of device studied, at least

Table 2. Photovoltaic Properties of Various CdS QDSCs Measured under the Illumination of One Sun[a]

sample	V_{oc} (V)	J_{sc} (mA/cm^2)	FF	η (%)
N-6	0.50	3.85	0.42	0.82
N-12	0.53	6.54	0.41	1.44
N-24	0.49	7.76	0.40	1.53
C-6	0.53	7.02	0.45	1.68
C-12	0.54	9.49	0.42	2.15
C-24	0.43	4.58	0.43	0.84

[a]AM 1.5, 100 mW/cm^2.

three identical samples were fabricated to check the reproducibility of cell performance (see Table S1 of the Supporting Information for a detailed discussion of reproducibility employing samples N-12 and C-12 as examples). As shown in Table 2, the changes in V_{oc} and FF were not large. However, a significant change in J_{sc} can be seen for the N and C series for different numbers of SILAR cycles. As for DSCs, the amount of dye loaded on the TiO_2 electrode predominantly affects the photocurrent density.[41,42] This is also the case for QDSCs, where QDs take the place of dye molecules. Therefore, the performance of a QDSC is very much dependent on the number of SILAR cycles employed to deposit the QDs. With increasing number of SILAR cycles, both the coverage ratio of CdS on the TiO_2 and the thickness of the CdS layer increase. Such an incremental increase in the CdS QD loading leads to more excited electrons under the same illumination, which contributes to the photocurrent. Figure S4b (Supporting Information) shows the dependence of the photocurrent density on the amount of QDs loaded on the TiO_2 films. A small amount of CdS QDs incorporated on the TiO_2 film results in a small photocurrent density, along with a small photocurrent and a poor cell performance, for example, for sample N-6. However, an overload of CdS QDs on the TiO_2 film also results in low cell performance, possibly for the reason of blocking of the mesopores, which leads to a decrease of the QD/electrolyte contact area and unfavorable electron transport at the TiO_2/QD/electrolyte interface. At the same time, it would be difficult for electrons to transfer from CdS to TiO_2 in an excessively thick CdS layer because of the increased diffusion distance and injection time.[43,44] This might explain the decrease in the efficiency and photocurrent density of sample C-24, the morphology of which (Figure 1f) indicates that the pores of the TiO_2 film are largely blocked. The highest photocurrent density of 9.49 mA/cm^2 was obtained in the QDSC based on the C-12 photoanode, implying an optimal amount of CdS QDs forming a well-distributed layer on the TiO_2 film. In contrast, the N series, that is, the electrodes that employed $Cd(NO_3)_2$ as the Cd^{2+} source, presented a much slower increase in the photocurrent density and efficiency with the growth of CdS QDs in comparison with the C series prepared using $Cd(Ac)_2$; more SILAR cycles, even as many as 24, did not result in better cell performance. The cell delivered the best power conversion efficiency of 2.15% for C-12, which was nearly a 40% enhancement compared to that for N-12, which was prepared with the same number of SILAR cycles.

These observations demonstrate that $Cd(Ac)_2$ precursor is more effective than $Cd(NO_3)_2$ for CdS QD deposition on TiO_2. A high deposition rate favors the ready formation of a conformal CdS QD layer coating on TiO_2, as the nucleation and growth of CdS QDs can be finished in a very short period of time, and therefore can facilitate electron injection from the QDs to the TiO_2. Good contact between the CdS and TiO_2 is important to enhance the charge separation.[45,46] The large short-circuit current and high efficiency of the cells prepared using $Cd(Ac)_2$ as the precursor should be ascribed to the formation of good contact between the CdS QDs and the TiO_2 layer because of the high deposition rate.[46,47] Such a superior interface between TiO_2 and CdS can inhibit the interfacial recombination arising from injected electrons diffusing from TiO_2 into the electrolyte.[45,46,48] In contrast, for $Cd(NO_3)_2$ precursor, because it takes much longer for the CdS QDs to adsorb onto the TiO_2 films, more surface defects of QDs might be produced during this process and, thus, cause increased carrier recombination, lowering the cell performance.[46,48] The Mora-Seró group reported increased injection efficiency and reduced surface defects based on ultrafast carrier dynamics and surface photovoltage spectroscopy when acetate precursor was employed instead of nitrate precursor, which supports our conclusion.[33] In addition, because of the porous structure of TiO_2 films, the pores might be easily blocked by QDs in the case of a time-consuming process. In other words, the excess of QDs adsorbed later might not be able to deposit into the inner pores inside the TiO_2 film in view of the channel obstruction during a long-term deposition. This could explain why the efficiency for the N series could not be increased substantially for large numbers of SILAR cycles and why the cell performance of C-6, with only six SILAR cycles, was better than the cell performances of all of the N series, even though the QD amount adsorbed for N-24 was larger than the amount adsorbed for C-6.

Figure 5 compares the IPCE curves of QDSCs based on N-12 and C-12 electrodes. It can be seen that the overall

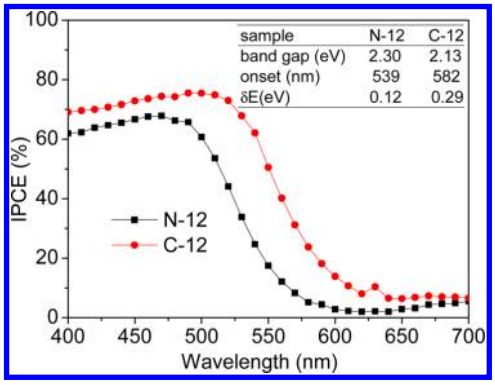

Figure 5. IPCE curves of the N-12 and C-12 electrodes measured as functions of wavelength. Inset: Band gaps, onsets, and band-gap shifts of CdS QDs obtained from IPCE curves.

photoresponse matches well with the absorption features, with the photocurrent onsets directly correlated with the absorption onsets. C-12 exhibited a higher IPCE than N-12 throughout the entire spectrum, resulting in a high photocurrent density (see the Supporting Information for a detailed calculation of the photocurrent density from the IPCE curves). The maximum IPCE of C-12 reached as high as 75% at a wavelength of ~490 nm. Band gaps can also be calculated from the spectral

dx.doi.org/10.1021/jp410615b | J. Phys. Chem. C 2013, 117, 26948−26956

response by extrapolating the square of the photocurrent (equivalent to IPCE[2]) to zero photocurrent.[49] The results are included in the inset of Figure 6. The values of the band gaps

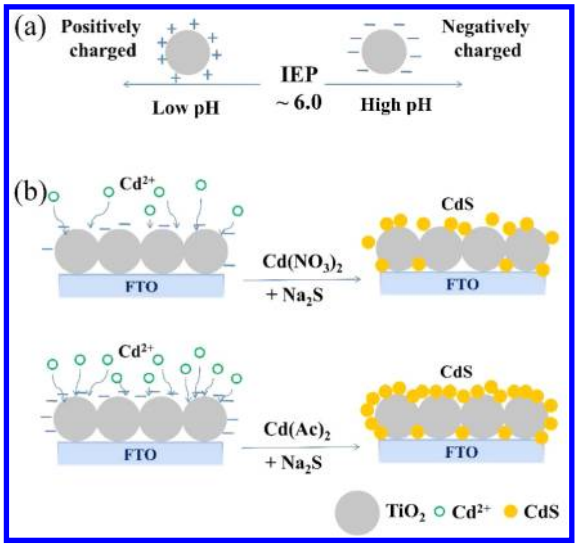

Figure 6. Schematic diagrams of (a) the surface charge of TiO_2 as a function of solution pH and (b) the deposition processes of CdS QDs on TiO_2 films using $Cd(NO_3)_2$ and $Cd(Ac)_2$ methanol solutions as cationic precursors. IEP stands for the isoelectric point.

show good agreement with those estimated from the optical spectral response. The photovoltaic properties reveal that the anomalous red shift of the absorption edge indeed contributes to the photoresponse at longer wavelengths, which results in a marked enhancement in the solar power conversion efficiency. In the literature, there are also a few examples of anomalous red shifts in the photocurrent response of cells based on SILAR-adsorbed CdS QDs on mesoporous TiO_2 or ZnO.[18,19,35,37,39,40,50] Such a pronounced red shift, which lowers the effective band gap of the QD-sensitized TiO_2 photoanode, broadens the absorption range of the solar spectrum, and thus, to some extent, makes up for the limited photoactive region of CdS (2.42 eV), is greatly beneficial for solar energy utilization.

The exact causes of the different deposition rates obtained using different Cd^{2+} precursors are still unclear at this stage. However, in our experiments, we observed that $Cd(NO_3)_2$ and $Cd(Ac)_2$ dissolved in methanol resulted in different acid−base properties. $Cd(NO_3)_2$ is a strong acid and weak base salt, whereas $Cd(Ac)_2$ is a weak acid and mild base salt. A higher pH value would be expected in $Cd(Ac)_2$ methanol solution than in $Cd(NO_3)_2$ methanol solution. Although dissolved in methanol solution, some water of crystallization existed in the $Cd(NO_3)_2\cdot 4H_2O$ and $Cd(Ac)_2\cdot 2H_2O$ used. Indeed, these two precursors presented noticeable difference in their pH values, ~6.1 for $Cd(NO_3)_2$ and ~7.6 for $Cd(Ac)_2$ at the same concentration of 0.1 M in the current investigation.

To investigate the influence of cadmium precursors on the deposition rate of CdS QDs on TiO_2 film, we performed some designed experiments in which the pH value of the Cd^{2+} precursor solution was changed. The results are listed in Table 3. The number of SILAR cycles was set to be 12. The relative QD contents were estimated according to the EDX analysis. Absorption onsets and effective band gaps were extrapolated from UV−vis absorption spectral responses. The deposition rate could be evaluated from the QD content and absorption onset. As we suspected that pH effects might be the main causes for the different deposition rates, acetic acid, nitric acid, and ammonia solutions were employed to adjust the pH of the precursor solution. When acetic acid was added to 0.1 M $Cd(NO_3)_2$ methanol solution ($HAc/Cd^{2+} \approx 1{:}1$, molar ratio), the amount of CdS QDs deposited on the TiO_2 film and the resulting photocurrent density both decreased as compared to the results for the original pure $Cd(NO_3)_2$ precursor listed in Table 3, indicating a decreased deposition rate as the pH dropped from ~6.1 to ~2.1. Similar results were obtained upon the addition of nitric acid to $Cd(Ac)_2$ methanol solution. In contrast, when ammonia solution was added to both the $Cd(NO_3)_2$ and $Cd(Ac)_2$ precursors ($NH_3\cdot H_2O/Cd^{2+} \approx 1{:}1$, molar ratio), the deposition rate of CdS QDs was significantly increased in the case of the $Cd(NO_3)_2$ precursor, as the pH increased to 7.7 from 6.1. For the $Cd(Ac)_2$ precursor, no appreciable enhancement in the deposition rate was observed as the pH increased from ~7.6 to ~8.8. These results suggest that the deposition of CdS QDs increases with increased pH but reaches saturation at pH ~8.0. See Figure S5 in the Supporting Information for a detailed study of the dependence of the deposition rate on the precursor pH. It is worth mentioning that the addition of ammonia to $Cd(NO_3)_2$ methanol solution created $Cd(OH)_2$ white precipitates in the precursor, whereas no precipitates were observed for $Cd(Ac)_2$ methanol precursor.

Although the exact mechanism by which the deposition rate of CdS QDs on TiO_2 films is closely associated with the pH of the precursor is not known, a varied surface charge on TiO_2 might be a response. When nanoparticles are dispersed in an aqueous solution or polar solvent or electrolyte, surface ionization and the adsorption of cations or anions would result in the generation of a surface charge and the development of an electric potential between the nanoparticle surface and the bulk of the dispersion medium.[51,52] For TiO_2 nanoparticles

Table 3. Summary of the Results of Control Experiments with Changing Recipes of Cationic Precursor Solutions for CdS QDs Deposited for 12 SILAR Cycles

cationic precursor	pH	content (%)	absorption onset (nm)	band gap (eV)	J_{sc} (mA/cm^2)	η (%)
$Cd(NO_3)_2$	~6.1	3.65	537	2.31	6.54	1.44
$Cd(Ac)_2$	~7.6	11.39	590	2.10	9.49	2.15
$Cd(NO_3)_2$+HAc	~2.5	1.14	528	2.35	3.85	0.91
$Cd(Ac)_2$+HNO_3	~6.4	7.15	571	2.17	7.25	1.60
$Cd(NO_3)_2$+$NH_3\cdot H_2O$	~7.7	11.68	591	2.10	9.18	1.97
$Cd(Ac)_2$+$NH_3\cdot H_2O$	~8.8	11.81	592	2.09	9.42	2.01
$Cd(NO_3)_2$+$Mn(Ac)_2$	~6.8	9.05	574	2.16	9.47	2.02
$Cd(NO_3)_2$+$Mn(NO_3)_2$	~6.0	3.66	540	2.30	6.32	1.39

dx.doi.org/10.1021/jp410615b | J. Phys. Chem. C 2013, 117, 26948−26956

immersed in aqueous solution, in general, their surface is covered by hydroxyl groups, according to the reaction

$$Ti^{IV} + H_2O \rightarrow Ti^{IV}{-}OH + H^+ \quad (2)$$

Once the solution pH changes, the surface charge of TiO_2 will be affected by the reactions occurring on the particle surface, such as

$$Ti^{IV}{-}OH + H^+ \rightarrow Ti^{IV}{-}OH_2^+ \quad (3)$$

$$Ti^{IV}{-}OH \rightarrow Ti^{IV}{-}O^- + H^+ \quad (4)$$

The surface charge can be evaluated from the zeta potential. The pH at which the surface of nanoparticles is neutral is defined as the isoelectric point (IEP), where the zeta potential equals zero.[51] The IEP for TiO_2 nanoparticles was reported to be $pH_{IEP} \approx 6.0$.[53−56] As illustrated by the schematic diagram of the surface charge of TiO_2 as a function of solution pH in Figure 6a, when the pH is below pH_{IEP}, there will be a positive surface charge and a positive zeta potential (eq 3). However, when the pH is greater than pH_{IEP}, a negative surface charge and negative zeta potential would be developed (eq 4).[52,53,57] Similar reactions would occur when TiO_2 was immersed in $Cd(NO_3)_2$ and $Cd(Ac)_2$ methanol precursor solutions (as illustrated in Figure 6b). As the $Cd(Ac)_2$ precursor exhibits a higher pH than the $Cd(NO_3)_2$ precursor, the TiO_2 surface would become more negatively charged for the film dipped in $Cd(Ac)_2$ precursor and, thus, have a higher driving force for the adsorption of Cd^{2+} ions. Consequently, when the TiO_2 films were successively dipped into Na_2S solution, allowing S^{2-} to react with the preadsorbed Cd^{2+}, a larger amount of CdS QDs was generated on the TiO_2 film dipped in $Cd(Ac)_2$ precursor. In other words, a much higher deposition rate of CdS QDs on the TiO_2 film can be achieved using $Cd(Ac)_2$ as the cationic precursor compared to $Cd(NO_3)_2$.

It should be noted that, after several cycles of SILAR deposition of CdS onto the TiO_2 surface, a portion of the subsequent layer of CdS would be deposited on the preadsorbed CdS surface, not only on the TiO_2 surface. Similar interpretations concerning the surface charge can also be made in this case. In the literature, the reported pH_{IEP} values are 5.5[58] and 3.7.[59] Despite the difference in values, it is considered that a high pH will also lead to a more negatively charged preadsorbed CdS surface, which contributes to the effective adsorption of Cd^{2+} ions in the precursor and, ultimately, results in a high deposition rate of CdS.

A study reported by Santra and Kamat supports the conclusion that acetate ligand provides better QD deposition than nitrate ligand.[27] They studied a strategy to boost the efficiency of QDSCs through Mn^{2+} doping of CdS. In their experiments, $Cd(NO_3)_2$ methanol solution (0.1 M) was used for CdS deposition, and $Mn(Ac)_2$ solution (0.075 M) was admixed with $Cd(NO_3)_2$ solution to incorporate Mn^{2+} into CdS, enabling the formation of Mn-doped-CdS QDSCs. Nearly 55% enhancement in the power conversion efficiency was achieved with a red shift of up to 50 nm in the absorption onset reported for Mn-doped-CdS as compared to undoped CdS. Our verification experimental results are reported in Table 3. As shown, adding $Mn(Ac)_2$ to $Cd(NO_3)_2$ precursor ($Mn^{2+}/Cd^{2+} \approx 1{:}10$, molar ratio) substantially increased the CdS deposition rate and red-shifted the absorption onset compared to the original $Cd(NO_3)_2$ precursor, and an improved QDSC performance of 2.02% (40% higher than the undoped performance) was obtained. However, when $Mn(Ac)_2$ was replaced by $Mn(NO_3)_2$ and admixed with $Cd(NO_3)_2$ precursor ($Mn^{2+}/Cd^{2+} \approx 1/10$, molar ratio), no obvious change in the amount of QDs deposited was found, as presented in Table 3. These observations are in good agreement with our suggestion that the acetate ligand can improve QD deposition and thus contribute to improved solar cell performance.

4. CONCLUSIONS

The present work has demonstrated that precursors have noticeable influences on the synthesis and assembly of QDs on photoanode films by the SILAR method for QDSCs. Further studies revealed that the pH value of the precursor solution is likely to determine the deposition rate and, consequently, to affect the amount of QDs deposited on the photoanode. A QDSC fabricated with CdS QDs deposited on TiO_2 mesoporous film using $Cd(Ac)_2$ as the Cd^{2+} precursor exhibited a power conversion efficiency as high as 2.15%, achieving nearly 40% enhancement compared to that obtained using $Cd(NO_3)_2$ for the same number (i.e., 12) of SILAR cycles. This effect is mainly attributed to the rapid deposition of QDs on TiO_2 films provided by the $Cd(Ac)_2$ precursor, which has a higher pH value. The cationic precursor selected to deposit CdS QDs by SILAR has a dramatic effect on the QDSC performance. An increased amount of QDs was found to be accompanied by an increasing degree of red shift of the absorption edge. An apparent anomalous red-shift phenomenon, not explicitly mentioned in most of the literature, was observed for CdS-QD-deposited TiO_2 films in our study. The combination of an increased amount of QDs and a broadened absorption spectrum resulted in an appreciable enhancement of the power conversion efficiency for otherwise identical device configurations.

■ ASSOCIATED CONTENT

Supporting Information

EDX spectra and mapping image for a CdS-sensitized TiO_2 film. Picture showing differences in the colors of various films. Dependences of the band-gap red shift and photocurrent density on the amount of QDs loaded on the TiO_2 films. Reproducibility of the solar cell performance. Calculation of the photocurrent density from IPCE curves. Dependence of the deposition rate on the pH for $Cd(Ac)_2$-based cationic precursors. This material is available free of charge via the Internet at http://pubs.acs.org.

■ AUTHOR INFORMATION

Corresponding Author

*E-mail: gzcao@u.washington.edu. Tel.: 206-616-9084. Fax: 206-543-3100.

Notes

The authors declare no competing financial interest.

■ ACKNOWLEDGMENTS

We acknowledge Dr. Huanxin Ju for help in performing the IPCE measurements. This work was supported in part by the National Science Foundation (DMR 1035196), a University of Washington TGIF grant, and the Royalty Research Fund (RRF) from the Office of Research at the University of Washington. R.Z. also acknowledges a fellowship from the China Scholarship Council.

REFERENCES

(1) Grätzel, M. Solar Energy Conversion by Dye-Sensitized Photovoltaic Cells. *Inorg. Chem.* **2005**, *44*, 6841−6851.
(2) Grätzel, M. Photoelectrochemical Cells. *Nature* **2001**, *414*, 338−344.
(3) Zhang, Q. F.; Chou, T. R.; Russo, B.; Jenekhe, S. A.; Cao, G. Z. Polydisperse Aggregates of ZnO Nanocrystallites: A Method for Energy-Conversion-Efficiency Enhancement in Dye-Sensitized Solar Cells. *Adv. Funct. Mater.* **2008**, *18*, 1654−1660.
(4) Zhang, Q. F.; Chou, T. R.; Russo, B.; Jenekhe, S. A.; Cao, G. Z. Aggregation of ZnO Nanocrystallites for High Conversion Efficiency in Dye-Sensitized Solar Cells. *Angew. Chem., Int. Ed.* **2008**, *47*, 2402−2406.
(5) Tian, J. J.; Zhang, Q. F.; Uchaker, E.; Liang, Z. Q.; Gao, R.; Qu, X. H.; Zhang, S. G.; Cao, G. Z. Constructing ZnO Nanorod Array Photoelectrodes for Highly Efficient Quantum Dot Sensitized Solar Cells. *J. Mater. Chem. A* **2013**, *1*, 6770−6775.
(6) Tian, J. J.; Zhang, Q. F.; Zhang, L. L.; Gao, R.; Shen, L. F.; Zhang, S. G.; Qu, X. H.; Cao, G. Z. ZnO/TiO_2 Nanocable Structured Photoelectrodes for CdS/CdSe Quantum Dot Co-Sensitized Solar Cells. *Nanoscale* **2013**, *5*, 936−943.
(7) Burschka, J.; Pellet, N.; Moon, S.-Jin.; Humphry-Baker, R.; Gao, P.; Nazeeruddin, M. K.; Grätzel, M. Sequential Deposition as a Route to High-Performance Perovskite-Sensitized Solar Cells. *Nature* **2013**, *499*, 316−319.
(8) Gonzalez-Pedro, V.; Xu, X.; Mora-Seró, I.; Bisquert, J. Modeling High-Efficiency Quantum Dot Sensitized Solar Cells. *ACS Nano* **2010**, *4*, 5783−5790.
(9) Zhu, G.; Pan, L.; Xu, T.; Sun, Z. CdS/CdSe-Cosensitized TiO_2 Photoanode for Quantum-Dot-Sensitized Solar Cells by a Microwave-Assisted Chemical Bath Deposition Method. *ACS Appl. Mater. Interfaces* **2011**, *3*, 3146−3151.
(10) Tian, J. J.; Gao, R.; Zhang, Q. F.; Zhang, S. G.; Li, Y. W.; Lan, J. L.; Qu, X. H.; Cao, G. Z. Enhanced Performance of CdS/CdSe Quantum Dot Cosensitized Solar Cells via Homogeneous Distribution of Quantum Dots in TiO_2 Film. *J. Phys. Chem. C* **2012**, *116*, 18655−18662.
(11) Yang, Z.; Zhang, Q. F.; Xi, J. T.; Park, K.; Xu, X. L.; Liang, Z. Q.; Cao, G. Z. CdS/CdSe Co-Sensitized Solar Cell Prepared by Jointly Using Successive Ion Layer Absorption and Reaction Method and Chemical Bath Deposition Process. *Sci. Adv. Mater.* **2012**, *4*, 1−5.
(12) Chang, C. H.; Lee, Y. L. Chemical Bath Deposition of CdS Quantum Dots onto Mesoscopic Films for Application in Quantum-Dot-Sensitized Solar Cells. *Appl. Phys. Lett.* **2007**, *91*, 053503.
(13) Lin, S. C.; Lee, Y. L.; Chang, C. H.; Shen, Y. J.; Yang, Y. M. Quantum-Dot-Sensitized Solar Cells: Assembly of CdS-Quantum-Dots Coupling Techniques of Self-Assembled Monolayer and Chemical Bath Deposition. *Appl. Phys. Lett.* **2007**, *90*, 143517.
(14) Sun, W. T.; Yu, Y.; Pan, H. Y.; Gao, X. F.; Chen, Q.; Peng, L. M. CdS Quantum Dots Sensitized TiO_2 Nanotube-Array Photoelectrodes. *J. Am. Chem. Soc.* **2008**, *130*, 1124−1125.
(15) Kim, J.; Choi, H.; Nahm, C.; Moon, J.; Kim, C.; Nam, S.; Jung, D. R.; Park, B. The Effect of a Blocking Layer on the Photovoltaic Performance in CdS Quantum-Dot-Sensitized Solar Cells. *J. Power Sources* **2011**, *196*, 10526−10531.
(16) Panigrahi, S.; Basak, D. Morphology Driven Ultraviolet Photosensitivity in ZnO−CdS Composite. *J. Colloid Interface Sci.* **2011**, *364*, 10−17.
(17) Lee, Y. L.; Lo, Y. S. Highly Efficient Quantum-Dot-Sensitized Solar Cell Based on Co-Sensitization of CdS/CdSe. *Adv. Funct. Mater.* **2009**, *19*, 604−609.
(18) Tak, Y.; Hong, S. J.; Lee, J. S.; Yong, K. Fabrication of ZnO/CdS Core/Shell Nanowire Arrays for Efficient Solar Energy Conversion. *J. Mater. Chem.* **2009**, *19*, 5945−5951.
(19) Jung, S. W.; Kim, J. H.; Kim, H.; Choi, C. J.; Ahn, K. S. CdS Quantum Dots Grown by in Situ Chemical Bath Deposition for Quantum Dot-Sensitized Solar Cells. *J. Appl. Phys.* **2011**, *110*, 044313.
(20) Robel, I.; Subramanian, V.; Kuno, M.; Kamat, P. V. Quantum Dot Solar Cells. Harvesting Light Energy with CdSe Nanocrystals Molecularly Linked to Mesoscopic TiO_2 Films. *J. Am. Chem. Soc.* **2006**, *128*, 2385−2393.
(21) Shen, Q.; Kobayashi, J.; Diguna, L. J.; Toyoda, T. Effect of ZnS Coating on the Photovoltaic Properties of CdSe Quantum Dot-Sensitized Solar Cells. *J. Appl. Phys.* **2008**, *103*, 084304.
(22) Samadpour, M.; Giménez, S.; Boix, P. P.; Shen, Q.; Calvo, M. E.; Taghavinia, N.; Iraji zad, A.; Toyoda, T.; Míguez, H.; Mora-Seró, I. Effect of Nanostructured Electrode Architecture and Semiconductor Deposition Strategy on the Photovoltaic Performance of Quantum Dot Sensitized Solar Cells. *Electrochim. Acta* **2012**, *75*, 139−147.
(23) Plass, R.; Pelet, S.; Krueger, J.; Grätzel, M.; Bach, U. Quantum Dot Sensitization of Organic−Inorganic Hybrid Solar Cells. *J. Phys. Chem. B* **2002**, *106*, 7578−7580.
(24) Braga, A.; Giménez, S.; Concina, I.; Vomiero, A.; Mora-Seró, I. Panchromatic Sensitized Solar Cells Based on Metal Sulfide Quantum Dots Grown Directly on Nanostructured TiO_2 Electrodes. *J. Phys. Chem. Lett.* **2011**, *2*, 454−460.
(25) Tubtimtae, A.; Wu, K. L.; Tung, H. Y.; Lee, M. W.; Wang, G. J. Ag_2S Quantum Dot-Sensitized Solar Cells. *Electrochem. Commun.* **2010**, *12*, 1158−1160.
(26) Chen, C.; Xie, Y.; Ali, G.; Yoo, S. H.; Cho, S. O. Improved Conversion Efficiency of Ag_2S Quantum Dot-Sensitized Solar Cells Based on TiO_2 Nanotubes with a ZnO Recombination Barrier Layer. *Nanoscale Res. Lett.* **2011**, *6*, 462−470.
(27) Santra, P. K.; Kamat, P. V. Mn-Doped Quantum Dot Sensitized Solar Cells: A Strategy to Boost Efficiency over 5%. *J. Am. Chem. Soc.* **2012**, *134*, 2508−2511.
(28) Hossain, M. A.; Jennings, J. R.; Shen, C.; Pan, J. H.; Koh, Z. Y.; Mathews, N.; Wang, Q. CdSe-Sensitized Mesoscopic TiO_2 Solar Cells Exhibiting >5% Efficiency: Redundancy of CdS Buffer Layer. *J. Mater. Chem.* **2012**, *22*, 16235−16242.
(29) Lee, H.; Wang, M. K.; Chen, P.; Gamelin, D. R.; Zakeeruddin, S. M.; Grätzel, M.; Nazeeruddin, M. K. Efficient CdSe Quantum Dot-Sensitized Solar Cells Prepared by an Improved Successive Ionic Layer Adsorption and Reaction Process. *Nano Lett.* **2009**, *9*, 4221−4227.
(30) Niitsoo, O.; Sarkar, S. K.; Pejoux, C.; Rühle, S.; Cahen, D.; Hodes, G. Chemical Bath Deposited CdS/CdSe-Sensitized Porous TiO_2 Solar Cells. *J. Photochem. Photobiol. A* **2006**, *181*, 306−313.
(31) Norris, D. J.; Leschkies, K. S.; Divakar, R.; Basu, J.; Enache-Pommer, E.; Boercker, J. E.; Carter, C. B.; Kortshagen, U. R.; Aydil, E. S. Photosensitization of ZnO Nanowires with CdSe Quantum Dots for Photovoltaic Devices. *Nano Lett.* **2007**, *7*, 1793−1798.
(32) Gimenez, S.; Mora-Seró, I.; Macor, L.; Guijarro, N.; Lana-Villarreal, T.; Gomez, R.; Diguna, L. J.; Shen, Q.; Toyoda, T.; Bisquert, J. Improving the Performance of Colloidal Quantum-Dot-Sensitized Solar Cells. *Nanotechnology* **2009**, *20*, 295204.
(33) González-Pedro, V.; Sima, C.; Marzari, G.; Boix, P. P.; Giménez, S.; Shen, Q.; Dittrich, T.; Mora-Seró, I. High Performance PbS Quantum Dot Sensitized Solar Cells Exceeding 4% Efficiency: The Role of Metal Precursors in the Electron Injection and Charge Separation. *Phys. Chem. Chem. Phys.* **2013**, *15*, 13835−13843.
(34) de la Fuente, M. S.; Sánchez, R. S.; González-Pedro, V.; Boix, P. P.; Mhaisalkar, S. G.; Rincón, M. E.; Bisquert, J.; Mora-Seró, I. Effect of Organic and Inorganic Passivation in Quantum-Dot-Sensitized Solar Cells. *J. Phys. Chem. Lett.* **2013**, *4*, 1519−1525.
(35) Rabinovich, E.; Hodes, G. Effective Bandgap Lowering of CdS Deposited by Successive Ionic Layer Adsorption and Reaction. *J. Phys. Chem. C* **2013**, *117*, 1611−1620.
(36) Tong, H.; Umezawa, N.; Ye, J.; Ohno, T. Electronic Coupling Assembly of Semiconductor Nanocrystals: Self-Narrowed Band Gap to Promise Solar Energy Utilization. *Energy Environ. Sci.* **2011**, *4*, 1684−1689.
(37) Baker, D. R.; Kamat, P. V. Photosensitization of TiO_2 Nanostructures with CdS Quantum Dots: Particulate versus Tubular Support Architectures. *Adv. Funct. Mater.* **2009**, *19*, 805−811.
(38) Gao, R.; Wang, L.; Geng, Y.; Ma, B.; Zhu, Y.; Dong, H.; Qiu, Y. Effects of an Intercalation Nanocomposite at the Photoanode/Electrolyte Interface in Quasi-Solid Dye-Sensitized Solar Cells. *J. Phys. Chem. C* **2011**, *115*, 17986−17992.

(39) Vogel, R.; Pohl, K.; Weller, H. Sensitization of Highly Porous, Polycrystalline TiO_2 Electrodes by Quantum Sized CdS. *Chem. Phys. Lett.* **1990**, *174*, 241−246.
(40) Ardalan, P.; Brennan, T. P.; Lee, H. B. R.; Bakke, J. R.; Ding, I. K.; McGehee, M. D.; Bent, S. F. Effects of Self-Assembled Monolayers on Solid-State CdS Quantum Dot Sensitized Solar Cells. *ACS Nano* **2011**, *5*, 1495−1504.
(41) Barbe, C. J.; Arendse, F.; Comte, P.; Jirousek, M.; Lenzmann, F.; Shklover, V.; Grätzel, M. Nanocrystalline Titanium Oxide Electrodes for Photovoltaic Applications. *J. Am. Ceram. Soc.* **1997**, *80*, 3157−3171.
(42) Chou, T. P.; Zhang, Q. F.; Russo, B.; Fryxell, G. E.; Cao, G. Z. Titania Particle Size Effect on the Overall Performance of Dye-Sensitized Solar Cells. *J. Phys. Chem. C* **2007**, *111*, 6296−6302.
(43) Lin, S. C.; Lee, Y. L.; Chang, C. H.; Shen, Y. J.; Yang, Y. M. Quantum-Dot-Sensitized Solar Cells: Assembly of CdS-Quantum-Dots Coupling Techniques of Self-Assembled Monolayer and Chemical Bath Deposition. *Appl. Phys. Lett.* **2007**, *90*, 143517.
(44) Zhang, Q. X.; Zhang, Y. D.; Huang, S. Q.; Huang, X. M.; Luo, Y. H.; Meng, Q. B.; Li, D. M. Application of Carbon Counterelectrode on CdS Quantum Dot-Sensitized Solar Cells. *Electrochem. Commun.* **2010**, *12*, 327−330.
(45) Gopidas, K. R.; Bohorquez, M.; Kamat, P. V. Photophysical and Photochemical Aspects of Coupled Semiconductors: Charge-Transfer Processes in Colloidal Cadmium Sulfide−Titania and Cadmium Sulfide−Silver(I) Iodide Systems. *J. Phys. Chem.* **1990**, *94*, 6435−6440.
(46) Zhu, G.; Pan, L. K.; Xu, T.; Sun, Z. One-Step Synthesis of CdS Sensitized TiO_2 Photoanodes for Quantum Dot-Sensitized Solar Cells by Microwave Assisted Chemical Bath Deposition Method. *ACS Appl. Mater. Interfaces* **2011**, *3*, 1472−1478.
(47) Li, L.; Qian, H.; Ren, J. Rapid Synthesis of Highly Luminescent CdTe Nanocrystals in the Aqueous Phase by Microwave Irradiation with Controllable Temperature. *Chem. Commun.* **2005**, *4*, 528−530.
(48) Diguna, L. J.; Shen, Q.; Kobayashi, J.; Toyoda, T. High Efficiency of CdSe Quantum-Dot-Sensitized Inverse Opal Solar Cells. *Appl. Phys. Lett.* **2007**, *91*, 023116.
(49) Gärtner, W. W. Depletion Layer Photoeffects in Semiconductors. *Phys. Rev.* **1959**, *116*, 84−87.
(50) Seol, M.; Kim, H.; Tak, Y.; Yong, K. Novel Nanowire Array Based Highly Efficient Quantum Dot Sensitized Solar Cell. *Chem. Commun.* **2010**, *46*, 5521−5523.
(51) Kosmulski, M. *Surface Charging and Points of Zero Charge*; CRC Press: Boca Raton, FL, 2009.
(52) Stumm, W.; Morgan, J. J. *Aquatic Chemistry*; Wiley-Interscience: New York, 1996.
(53) Suttiponparnit, K.; Jiang, J. K.; Sahu, M.; Suvachittanont, S.; Charinpanitkul, T.; Biswas, P. Role of Surface Area, Primary Particle Size, and Crystal Phase on Titanium Dioxide Nanoparticle Dispersion Properties. *Nanoscale Res. Lett.* **2011**, *6*, 27.
(54) Jiang, J. K.; Oberdörster, G.; Biswas, P. Characterization of Size, Surface Charge, and Agglomeration State of Nanoparticle Dispersions for Toxicological Studies. *J. Nanopart. Res.* **2009**, *11*, 77−89.
(55) Kosmulski, M. pH-Dependent Surface Charging and Points of Zero Charge. IV. Update and New Approach. *J. Colloid Interface Sci.* **2009**, *337*, 439−448.
(56) Miyauchi, M.; Ikezawa, A.; Tobimatsu, H.; Irie, H.; Hashimoto, K. Zeta Potential and Photocatalytic Activity of Nitrogen Doped TiO_2 Thin Films. *Phys. Chem. Chem. Phys.* **2004**, *6*, 865−870.
(57) Davis, J. A.; James, R. O.; Leckie, J. O. Surface Ionization and Complexation at the Oxide/Water Interface: I. Computation of Electrical Double Layer Properties in Simple Electrolytes. *J. Colloid Interface Sci.* **1978**, *63*, 480−499.
(58) Liu, J. C.; Huang, C. P. Electrokinetic Characteristics of Some Metal Sulfide−Water Interfaces. *Langmuir* **1992**, *8*, 1851−1856.
(59) Matijević, E.; Wilhelmy, D. M. Preparation and Properties of Monodispersed Spherical Colloidal Particles of Cadmium Sulfide. *J. Colloid Interface Sci.* **1982**, *86*, 476−484.